

The marriage of plasmonics, magnetism, acoustics and ultrafast optics

Vasily V. Temnov

*Institut des Molécules et Matériaux du Mans, UMR CNRS 6283,
Université du Maine, 72085 Le Mans cedex, France*

(Dated: July 12, 2012)

Surface plasmon polaritons (SPP or SP) are electromagnetic waves propagating along metal dielectric interfaces and existing over a wide range of frequencies. They have become popular because of their sub-wavelength confinement and the possibility to perform ultrasensitive optical measurements. Driven by tremendous progress in nanofabrication techniques and ultrafast laser technologies the applications of SP nanooptics extend beyond the border of nanoplasmonics. Here we review how using novel hybrid multilayer structures combining different functionalities allows to develop active plasmonic devices and new metrologies. Magneto-plasmonics, acousto-plasmonics and generation of high-energy photoelectrons using ultrashort SP pulses represent a few examples how the combination of ideas developed in the individual subfields can be used to generate new knowledge suggesting plenty of exciting applications in nanophotonics.

Investigation of plasmonic devices beyond the diffraction limit [1] represents a topical research direction in active plasmonics with major progress reported on the development of SP-based amplifiers and lasers [2]. After the original theoretical proposal by Krasavin and Zheludev to use structural thermally induced phase transitions in gallium-coated plasmonic waveguides [3] many other ways to actively control SP propagation have been realized in the experiment including electro-optic effect in dielectric overlayers [4], optical excitation of semiconductor quantum dots [5, 6] or magnetization switching in magneto-plasmonic materials [7]. Whereas nanoplasmonics with quantum dots has been extensively discussed elsewhere [2, 8] here we review the progress in magneto-plasmonics, ultrafast acousto-plasmonic and magneto-acoustic interactions. This development is largely driven by continuously improving nanofabrication techniques and borrowing the ideas from other well-established research directions. Despite of being very different in nature these studies follow the same idea: to explore various light-matter interactions in metallic nanostructures at the true nanoscale, within the tiny skin depth of light at visible and near IR frequencies. Development of hybrid ultrafast nanophotonic devices for future telecommunication and data recording technologies represents the final goal of these research activities.

The basic knowledge of the spatial distribution of electromagnetic field at interfaces supporting propagating SP waves appears to be inevitably necessary to understand the underlying physics. A typical hybrid noble

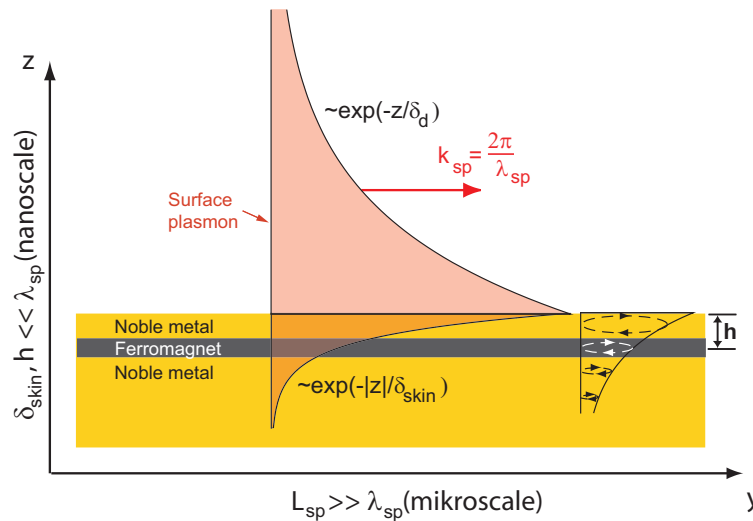


FIG. 1: **Surface plasmons in metal/ferromagnet/metal multilayer structures.** A few nanometers thin ferromagnetic layer integrated in the metal within SP skin depth δ_{skin} almost does not disturb the spatial distribution of SP intensity inside the metal and can be used to control SP propagation via magneto-optical effect in cobalt. Surface plasmon with frequency $\hbar\omega = 1.55$ eV (corresponding to $\lambda = 800$ nm optical wavelength in free space) at gold/air interface is characterized by SP wavelength $\lambda_{\text{sp}} = 794$ nm, propagation distance $L_{\text{sp}} = 45$ μm , skin depth $\delta_{\text{skin}} = 13$ nm and decay length in air $\delta_d = 307$ nm. Dashed elliptical contours show trajectories of electrons moving in SP electric field.

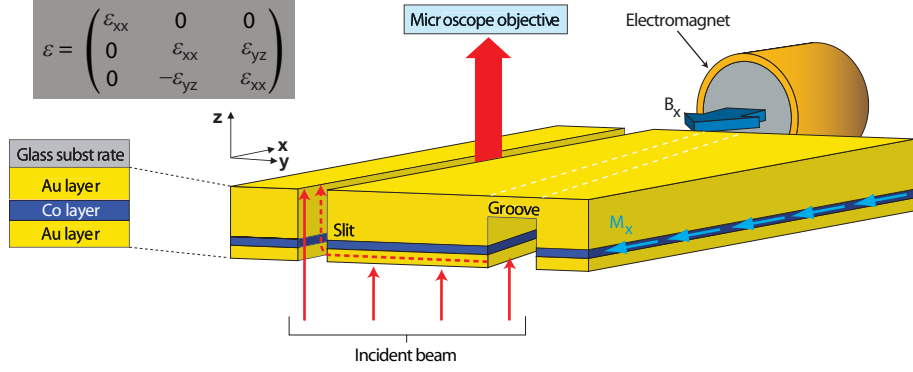


FIG. 2: **Active magneto-plasmonics.** The magnitude of SP wavevector $k_{sp}(M_x)$ in a magneto-plasmonic Au/Co/Au trilayer changes as the in-plane magnetization M_x in cobalt is periodically switched by a weak (20 mT) external magnetic field of an electromagnet, thus shifting the optical phase in the plasmonic interference arm by $\delta k_{mp}D=0.02$ rad. Figure adopted with permission from ref. [9].

metal/ferromagnet/noble metal multilayer structure, to be discussed within the framework of magneto-plasmonics, is sketched in Fig. 1. The strong dielectric contrast at metal-air interface characterized by a large negative real part of metal dielectric function determines the spatial distribution of exponentially decaying SP electric field. Due to a much weaker dielectric contrast between the adjacent metals the spatial distribution of SP intensity in a metal/ferromagnet/metal trilayer exhibits only minor deviations as compared to SP at single metal-air interface ($|E_y|^2$ is shown in Fig. 1) [7]. In order to be able to efficiently interact with surface plasmons, the ferromagnetic layer must have substantial overlap with the electric field of surface plasmon. SP intensity penetration (skin) depth δ_{skin} inside the metal is of the order of 10 nm in the visible and near infrared frequency range dictating the ultimate nano-scale for hybrid noble metal/ferromagnet multilayers characterized by $h \sim \delta_{skin} \ll \lambda_{sp} \simeq \lambda$. SP decay length δ_d on the dielectric side is a fraction of optical wavelength λ and is thus significantly larger as compared to the skin depth.

Strongly absorbing ferromagnetic metal layer introduces substantial losses - both due to large intrinsic absorption and possibly due to increased interface roughness. However, SP propagation distance in such hybrid structures usually remains large compared to optical wavelength: $L_{sp} \gg \lambda_{sp}$ (for example $L_{sp} = 10 \mu\text{m}$ for a Au/Co/Au structure with $h=8$ nm and 6 nm thickness of the cobalt layer [7]). This large propagation distance allows to design devices with plasmonic in- and out-couplers separated by large distance $D \sim L_{sp}$ of the order of at least a few microns and perform optical measurements with conventional optical microscopy techniques. Small external modulation of SP wave vector δk_{sp} or/and decay length δL_{sp} is accumulated over a large SP propagation distance and can be easily measured by surface plasmon interferometry or, to some extent, in Kretschmann configuration (see Box1).

A. Magneto-plasmonics

The idea to control the optical properties of SP using magnetic effects started with theoretical paper by Chiu and Quinn [10], who investigated the change in SP dispersion relation at an interface between vacuum and free-carrier metal induced by an external magnetic field. The Lorentz force acting on the electrons moving along the closed elliptical trajectories (dashed contours in Fig. 1) in the electric field of SP was shown to change the magnitude of SP wave vector. The largest change was predicted for in-plane magnetic field perpendicular to SP wave vector (in x-direction). Exploiting the high sensitivity of Kretschmann configuration Haefner and co-workers [11] observed this tiny effect in plasmonic free-carrier like metals Cu, Ag, Au and Al at relatively low external magnetic field $B = 200$ millitesla (mT). A good quantitative agreement was obtained for Ag and Au using simple free-electron (Drude) theory for the non-diagonal components of the linear dielectric permittivity tensor

$$\epsilon_{yz}^{Drude} = i \frac{\omega_c \omega_p^2}{\omega [(\omega + i/\tau_{Dr})^2 - \omega_c^2]}, \quad (1)$$

where $\omega_c = eB_x/m_{eff}$ is a cyclotron frequency (e - electron charge, m_{eff} - electron effective mass). Whereas expression (1) provided accurate results for Ag and Au, only order of magnitude agreement for Al and Cu was obtained. It was explained by possible contributions of interband transitions, which are disregarded in the Drude model. The magnitude of magneto-optic effect in diamagnetic noble metals $\epsilon_{yz}/\epsilon_{xx} \sim 10^{-7} B_x [\text{mT}]$ was found too small ruling out practical applications requiring reasonably low external magnetic fields.

Much larger magneto-optical effects with $\epsilon_{yz}/\epsilon_{xx} \sim 10^{-2}$ were found in ferromagnets. Modern energy-band theory calculations suggest that the magneto-optical properties in Fe, Ni and Co at visible frequencies are dominated by interband transitions, with $\epsilon_{yz} \propto M_x$ proportional to magnetization $M \sim 1$ Tesla in a ferromagnet [12]. Possible Drude-like contributions caused by the very same Lorentz force in a large built-in magnetic field of a ferromagnet $B_{eff} \propto M$ [13] are shown to contribute to the non-diagonal elements of dielectric permittivity only in the near-infrared frequency range (for photon energies below 1 eV in Fe)[12]. Since both interband and intraband (Drude) contributions scale linearly with M , optical measurements of the non-diagonal components are widely used to study magnetic properties of materials, including at ultrafast time scales.

Experiments with multilayer structures consisting of a thin ferromagnetic film sandwiched between two layers of noble metal in Kretschmann configuration demonstrated further increase of magneto-optical effects due to excitation of SP [14]. Systematic studies of Au/Co/Au trilayers with different geometric parameters showed that structures with a 6 nm thin cobalt layer gave maximum enhancement of magneto-plasmonic signal in Kretschmann configuration [15]. Another advantage of using thin ferromagnetic layers is that a small external magnetic field of the order of a few millitesla (mT) is sufficient to switch the in-plane magnetization. The magnitude of the switching field in single crystal samples drops below 1 mT for thin epitaxial iron films, one order of magnitude smaller than in polycrystalline samples, opening the door for practical applications [16].

Combined with SP interferometry these studies allowed to build a prototype of magneto-plasmonic device consisting of a tilted slit-groove microinterferometer milled by a focussed ion beam in the magneto-plasmonic Au/Co/Au (5 nm/6 nm/191 nm) multilayer structure [7]. The external magnetic field of an electromagnet switched the magnetization of the cobalt layer and thus changed the magnitude of SP wave vector. The relatively small magneto-plasmonic modulation of SP wavevector $\delta k_{mp}/k_{sp} \sim 10^{-4}$ was accumulated over a large propagation distance $D = 22 \mu\text{m}$ and produced a substantial shift of plasmonic interference fringes of 0.02 radian between two opposite magnetization directions. This phase shift could be further increased by covering the device with a thin layer of a high-index dielectric material [17], pointing towards future application as a magneto-plasmonic switch.

The magneto-plasmonic modulation of SP wave vector is ultimately sensitive to SP intensity at the location of a thin ferromagnetic layer. Therefore it can be used to measure the electric field distribution inside the metal with nanometer spatial resolution determined by the thickness of the magnetic (probe) layer. By varying the position h of a 6 nm thin cobalt layer the 13 nm skin depth of surface plasmon in gold was directly measured [7].

A slightly different version of magneto-plasmonic measurements was implemented in periodically perforated metal films covered with a layer of a ferromagnetic dielectric bismuth iron garnet [18]. Here, the ability to selectively modify SP wavevector at metal/magnetic dielectric interface not only confirmed the plasmonic origin of extraordinary high transmission [19] but also demonstrated a giant magneto-optical Kerr effect in transmission mode. In another experiment the surface-sensitive non-linear optical technique of magnetization-induced second harmonic generation revealed the direction of magnetization in nickel nanostructures, an effect interesting for magneto-plasmonic sensing applications [20]. The combination of magneto-plasmonic detection in a periodically oscillating magnetic field and Kretschmann geometry was shown to increase the detection sensitivity for biosensing applications [21] as compared to conventional SPR sensors [22].

One of the most intriguing questions concerns the maximum possible speed of all-optical modulation in nanophotonic devices and limiting time of magnetization reversal (switching) in magneto-plasmonic and, more generally, magneto-optical devices, which can be potentially used in new ultrafast telecommunication and data recording technologies. These questions have been tackled in various experiments combining magnetism, plasmonics with ultrafast optical measurements.

B. Ultrafast opto-plasmonic modulation

A modern version of femtosecond time-resolved measurements in a nanophotonic device was reported recently by MacDonald and co-workers [23], who have designed an ultrafast plasmonic light modulator (Fig. 3a). A pair of identical one-dimensional gratings was etched in silica and covered with aluminum film by thermal evaporation. A femtosecond laser pulse illuminated the first grating launching an ultrashort SP pulse, which propagated at aluminum-silica interface and was diffracted into free-space radiation by the second grating. An intense ultrashort control pump pulse was focused between the gratings and triggered diverse nonlinear optical phenomena in aluminum and, therefore, changed the optical absorption for ultrashort SP pulses. By varying the delay between the pump (control) and probe (signal) pulses the researchers demonstrated ultrafast plasmonic modulation of the decoupled signal on a sub-picosecond time scale opening the door to all-optical modulation rates in the THz frequency range. The origin of ultrafast sub-picosecond modulation in this device was attributed to the pump-induced third-order optical nonlinearity in the vicinity of interband transition in aluminum at $\lambda = 800$ nm [25] and possible contribution from transient grating effect originating from the interference between pump and SP pulses. A clean observation of transient grating effect

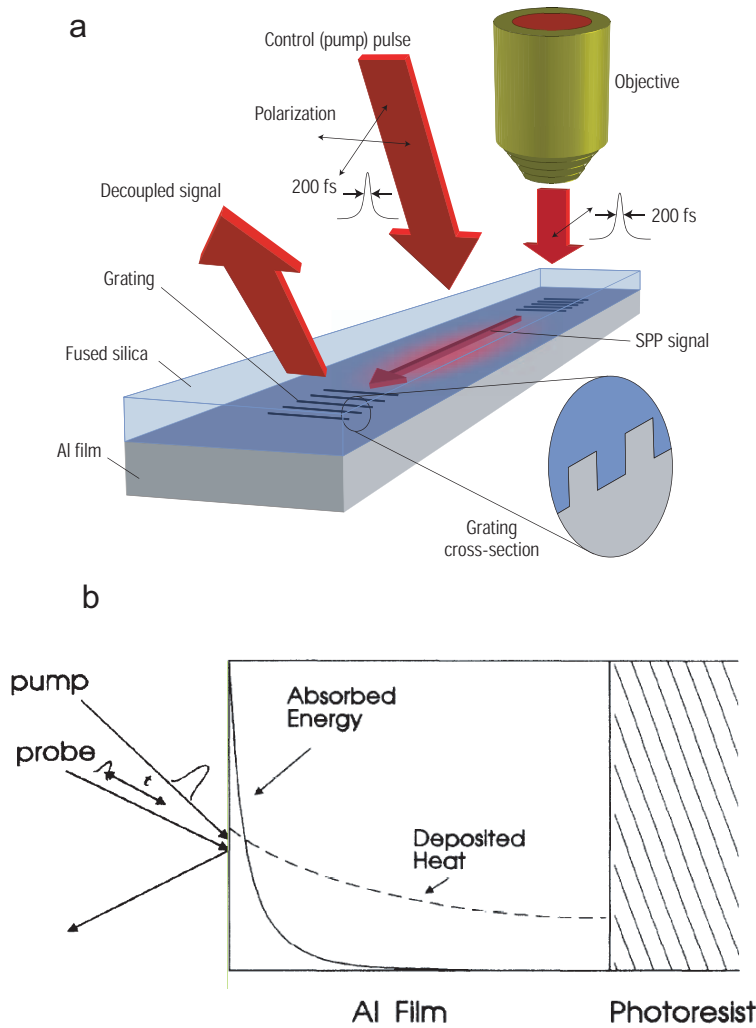


FIG. 3: **Ultrafast plasmonic modulation in fs-laser excited aluminum films.** **a**, The transmission of an ultrashort SP pulse propagating at Al/silica interface is perturbed by focussing an intense femtosecond control (pump) pulse between the gratings, which serve for SP in- and out-coupling. **b**, Efficient electron diffusion in plasmonic metals leads to much larger heat penetration depth as compared to the skin depth, where the energy of an intense femtosecond pump pulse is absorbed, the effect known from conventional time-resolved pump-probe reflectivity measurements. Figures reproduced with permission from: **a**, ref. [23]; **b**, ref. [24].

with surface plasmons was reported later in a different experiment on planar gold-air interface [26].

However, the device in Fig. 3a also showed much slower dynamics evident on the time-scale of tens of picoseconds. To explain these a variety of physical phenomena following the interaction of a femtosecond laser pulses with metal needs to be discussed in more detail [27]. An ultrashort laser pulse is absorbed by free carrier absorption creating a short-living distribution of non-equilibrium electrons. Electrons thermalize with each other through electron-electron collisions within at most a few hundreds of femtoseconds, with the longest electronic thermalization time of ~ 500 fs reported for gold [27]. After thermal equilibrium between the electrons is established, which can be adequately described by a high electron temperature, the transient state is still highly non-equilibrium because the electron temperature is still much higher than lattice temperature. Due to electron-phonon collisions hot electrons cool down and the lattice warms up until the common equilibrium temperature is established within a few picoseconds. This sequence of events in time domain is accompanied by diffusion of hot electrons in space, out of the skin depth where they originally absorbed laser energy. Later on, thermal expansion leads to the generation of coherent acoustic pulses [28] followed by cooling down of the lattice due to thermal diffusion on the time scale exceeding tens of picoseconds.

An elegant experiment exploiting thermo-acoustic generation as a probe of electronic heat diffusion depth in noble metals was reported by Tas and Maris [24]. For sufficiently thin samples, a situation sketched in Fig. 3b, the heat diffusion by hot electrons generated by the pump pulse leads to the nearly homogeneous heating of an aluminum film.

It resulted into the generation of the acoustic pulse at aluminum-photoresist interface caused by thermal expansion of aluminum. After propagation through the film at the speed of sound c_s , the acoustic strain pulse arrived at aluminum-air interface where it was detected by a time-delayed probe pulse via strain-induced transient reflectivity changes, a standard technique in picosecond ultrasonics [28].

C. Ultrafast acousto-plasmonics

It was demonstrated by van Exter and Lagendijk back in 1988 that SP excitation in Kretschmann geometry can greatly enhance the magnitude of pump-probe signals as compared to conventional reflectivity measurements [30]. A thin silver layer was excited through the glass prism by a picosecond pump pulse resulting into the homogenous heating through film depth $d = 45$ nm. The dynamics of thermal expansion governed by acoustic generation, propagation and reflection at silver-glass and silver-air interfaces caused the periodic expansion and contraction of silver layer at a frequency of 42 GHz= $c_s/(2d)$ determined by the acoustic round trip through the layer. Tiny acoustic modulation in lattice density changed the wavevector of time-delayed SP probe pulses resulting into drastic change of probe reflectivity in Kretschmann configuration. From the decay time of thermo-acoustic oscillations, which was mainly due to the finite (52%) acoustic reflection at silver-glass interface, the researchers were able to conclude that the intrinsic life time of longitudinal phonons in silver at 42 GHz largely exceeded 100 ps. Nowadays measurements of the mean free path (or lifetime) of high-frequency phonons in solids are found to be extremely important to understand thermal properties of the materials at the nanoscale driven by the interplay of ballistic and diffusive heat transport [31]. Similar fs-time-resolved experiments in thin gold and copper films [32, 33] revealed the contribution of short-living non-equilibrium electrons in the build up of mechanical stress driving the initial stage of thermo-acoustic expansion, in agreement with analogous measurements in plasmonic nanoparticles [34].

Despite of the appealing simplicity and high sensitivity of plasmonic pump-probe experiments in Kretschmann configuration their quantitative yield appeared to be rather limited. Very accurate time- and angular-dependent reflectivity measurements were necessary to reconstitute the dynamics of surface dielectric function [35]. Quantitative measurements can be performed by plasmonic pump-probe interferometry with femtosecond time resolution [29]. Figure 4b shows the experimental configuration of this technique adopted to acousto-plasmonic studies. In contrast to most previous measurements performed with a single polycrystalline metal layer on a dielectric substrate we used a Au/Co/sapphire structure with well-defined crystallographic (111) orientation of gold [36]. A 35 nm thick cobalt layer excited by an intense ultrashort laser pulse through sapphire substrate serves as an efficient and ultrafast opto-acoustic transducer. Due to much faster electron-phonon relaxation in ferromagnetic materials of the order of 0.2-0.3 ps [37] and much shorter electronic mean free path $l_e \sim 1$ nm [38] the hot electron diffusion is much less efficient than in noble metals characterized by $l_e \sim 40$ nm [39]. Therefore the heat penetration depth in ferromagnetic metals only slightly (typically by $\sim 50\%$) exceeds the skin depth for pump light [40]. Thermal expansion of fs-laser-heated cobalt layer generates an ultrashort acoustic strain pulse in both directions, into the gold layer and into the sapphire substrate. Very good acoustic impedance matching between three layers suppresses the acoustic reflection at gold/cobalt and cobalt/sapphire interfaces (both are about 10%) and the initial shape of a unipolar acoustic pulse follows the spatial profile of deposited heat in cobalt. Keeping in mind interesting nonlinear dynamics of ultrashort acoustic pulses observed in sapphire [41, 42] here we focus on the acousto-plasmonic effect in gold. The compressional acoustic pulse in gold $\eta(z, t) = (n_i(z, t) - n_i^0)/n_i^0$ creates a layer of higher ion density $n_i(z, t) > n_i^0$ and moving slowly at sound velocity $c_s = 3.45$ km/s. Due to the strong acoustic anisotropy in crystals the speed of sound in (111) direction is significantly higher than the value of 3.24 km/s in polycrystalline gold, averaged over different grain orientations. Since the stationary charge separation between the electrons and the ions in a metal may occur only within a tiny Debye radius $r_{\text{Debye}} \sim 10^{-3}$ nm, the spatial profile of electron density $n_e(z, t)$ exactly follows the ionic one: $n_e(z, t) = n_i(z, t)$. At 1.55 eV photon energy ($\lambda = 800$ nm) of probe pulses the dielectric function $\epsilon_m = \epsilon' + i\epsilon'' = -24.8 + 1.5i$ in gold is dominated by free-carrier contribution with $\epsilon' \simeq -\omega_p^2/\omega^2 \propto -n_e$. An ultrashort acoustic strain pulse creates a time-dependent spatial profile of the dielectric function $\epsilon'(z, t) = \epsilon'(1 + \eta(z, t))$ inside the metal, which modulates SP wavevector [29]

$$\delta k_{\text{sp}}(t) = \frac{k_0}{2|\epsilon_m|\delta_{\text{skin}}} \int \eta(z, t) \exp(-|z|/\delta_{\text{skin}}) \text{sgn}(z - c_s t) dz, \quad (2)$$

when the strain pulse arrives within SP skin depth. Here the $\text{sgn}(z - c_s t)$ function describes the transformation of the incident compressive pulse into the tensile one during the acoustic reflection at metal-air interface. Experimental acousto-plasmonic pump-probe interferogram in Fig. 4c demonstrates a pronounced transient shift of plasmonic fringes governing the acoustic reflection at gold-air interface. Application of standard interferometric analysis techniques and using expression (2) allows to reconstruct the acoustic pulse shape without using any fit parameters, see the acoustic

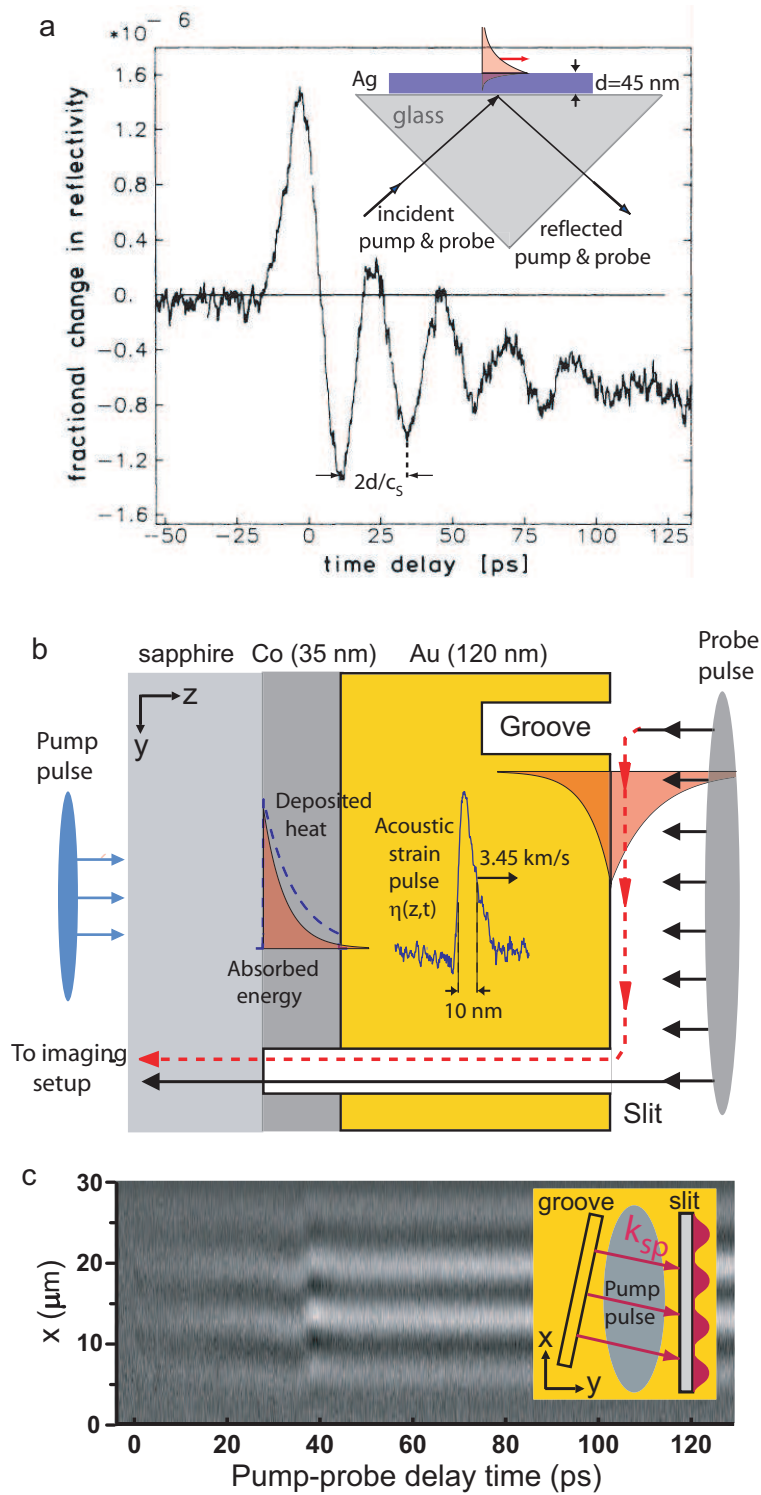


FIG. 4: **Ultrafast acousto-plasmonics.** **a**, Plasmonic pump-probe experiments in Kretschmann geometry allow for ultra-sensitive detection of coherent acoustic oscillations induced by thermal expansion of a 45 nm thin silver layer homogeneously heated by an ultrashort laser pulse. **b**, In hybrid acousto-plasmonic structures the thermal expansion of cobalt transducer excited by a femtosecond pump pulse at time zero launches an ultrashort acoustic pulse $\eta(z,t)$ propagating through gold at the speed of sound $c_s = 3.45$ km/s. **c**, After approximately 38 ps the acoustic reflection from gold-interface changes the wavevector of a time-delayed ultrashort SP probe pulse generating the acousto-plasmonic pump-probe interferogram in a tilted slit-groove arrangement. The 10 nm wide acoustic strain pulse in Fig. 4b has a duration of 3 ps and is reconstructed from transient phase shift in Fig. 4c. Measurements are performed by time-resolved SP interferometry [29]. Figure **a**, adopted with permission from ref. [30].

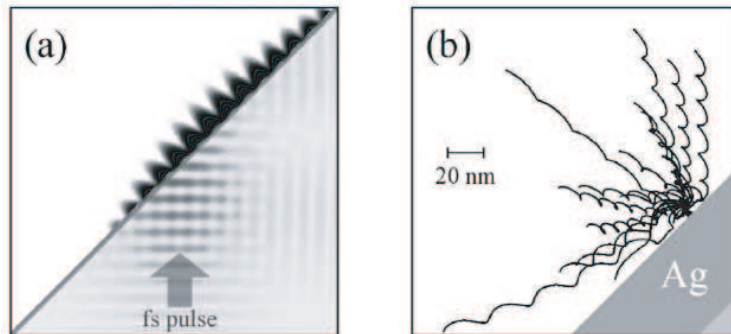


FIG. 5: **Generation and acceleration of high-energy photoelectrons with fs-laser pulses in Kretschmann geometry.** **a**, The intensity of incident fs-laser pulse is strongly enhanced as it is converted into an ultrashort SP in a 50 nm thin silver layer in Kretschmann configuration. **b**, Calculated trajectories of photoelectrons accelerated away from the surface in the field of intense ultrashort SP pulse. Figures reproduced with permission from ref. [49].

pulse in Fig. 4b. Acoustic pulse width of 10 nm (FWHM) corresponds to pulse duration of 3 ps. The temporal profile of the acoustic pulse is measured with 600 fs time resolution, which is limited by nanometer surface roughness (~ 2 nm RMS) implying random distribution of acoustic arrival times at gold-air interface. The peak strain of presented acoustic pulse is $\eta_{max} = 2.5 \times 10^{-3}$ although much higher strain amplitudes up to 0.01 (corresponding to uniaxial stress of ~ 2 GPa) and leading to the non-linear acoustic propagation effects in gold were observed in the same sample [36]. Application of 1%-strain in gold shifts the plasmonic fringes by ~ 0.01 radian, similar to the magneto-plasmonic switch in Fig. 2. The time scale of ultrafast acousto-plasmonic modulation is limited by the acoustic travel time through the skin depth $\tau_{skin} = \delta_{skin}/c_s = 3.8$ ps (in gold), although much shorter pulses can be detected.

Being ultimately sensitive to free-carrier density the plasmonic detection represents a quantitative technique which is complimentary to the acoustic characterization via pump-probe reflectivity measurements [28] and transient surface deformations with common-path interferometry [42]. Indeed, particularly large pump-probe signals observed in metals in the vicinity of interband transitions [28] show drastic change in shape due to strong and often unknown wavelength-dependence of photoelastic coefficients $d\sqrt{\epsilon_m}/d\eta$ [43]. An encouraging way to obtain photo-elastic coefficients in noble metals is provided by recent studies of tiny plasmonic nanoparticles. Large surface tension in nanoparticles with nanometer radius leads to their contraction and changes the electron density inducing the blue shift in plasma frequency [44]. However, if the optical wavelength falls within the region of interband transitions, lattice contraction also changes the dielectric function of core electrons according to simple Clausius-Mosotti formula inducing the red-shift of SP resonance frequency [45]. Although this theory has not been rigorously compared with experimental data in picosecond ultrasonics, the competition of intraband (free-carrier) and interband contributions provides a reasonable explanation for disappearance of acousto-optic pump-probe signals in Cu and Al in the vicinity of interband transitions (at $\lambda=575$ nm and 850 nm, respectively) [46]. In case the reliable tabulated values for photoelastic coefficients in noble metals become available simple pump-probe reflectivity measurements may be able to provide quantitative characterization of ultrashort acoustic strain pulses as well. Extraction of acoustic pulse shapes from much more complicated time-resolved interferometry measurements also depends on photo-elastic coefficients, although under some specific conditions the measured optical phase $\delta\phi(t) = \delta\phi_{metal}(t) + \delta\phi_{surface}(t)$ is dominated by the second well-defined term $\delta\phi_{surface}(t) = (4\pi/\lambda)\delta z(t)$ caused by transient surface displacement $\delta z(t)$ [42, 47].

SP propagation along the surface is usually not affected by small transient surface deformation $\delta z(y, t)$. However, spatially periodic modulation $\delta z(y) = \delta \sin(2\pi y/\Lambda_G)$ along SP propagation direction y may serve as a grating for phase-matched in- and out-coupling of SP into free space radiation. Periodic grating at gold-air interface with amplitude $\delta \sim 1$ nm and $\Lambda_G = 7.6 \mu\text{m}$ induced by surface acoustic wave at 480 MHz frequency was shown to convert near-infrared light into SP with $\sim 10^{-4}$ efficiency [48].

D. High-energy photoelectron generation with femtosecond SP pulses

Another interesting application in ultrafast plasmonics reveals the possibility to generate high-energy photoelectrons at metal-vacuum interface using femtosecond SP pulses. This phenomenon was observed both with an amplified high-power 250 kHz laser system [50] and a non-amplified Ti:sapphire oscillator operating at high repetition rate of 80 MHz [49]. In these experiments femtosecond laser pulses were used to illuminate a 50 nm thin silver layer

in Kretschmann geometry (Fig. 5a). The combination of ultrashort pulse duration, intrinsic field enhancement in Kretschmann geometry and sub-wavelength confinement of SP intensity exponentially decaying within $\delta_d = 240$ nm allowed to reach extremely high gradient of electric field of 8×10^{13} V/cm² in the direction normal to the surface [49]. Figure 5b shows typical calculated traces of photoelectrons, which were born at random times and with random initial velocities in three-photon-photoemission process and accelerated away from the surface on quivering trajectories gaining the kinetic energy up to 0.4 keV [49]. Most recent experiments with amplified phase-stabilized laser pulses allowed to reach electron kinetic energies up to 100 keV and also revealed the importance of nanoscale surface roughness affecting the photoemission process of individual electrons [51].

Photoemission and acceleration of photoelectrons in SP electric field generates an ultrashort pulse of electric current in the direction normal to the surface. SP-mediated THz radiation emitted by this current was observed very recently in periodic gratings on gold and silver surfaces [52]. The dependence of THz intensity on the angle of incidence and polarization of intense femtosecond pump pulses clearly demonstrated the dominating role of SP in THz generation. These experiments explain the diversity of published experimental data (see references in [52]) and undermount the hypothesis about the role of non-equilibrium ballistic electron transport, which was suggested to explain the non-local character of THz generation in thin gold films [53].

E. Ultrafast laser-induced magnetization dynamics

Besides the complex spatio-temporal dynamics of electrons and phonons in noble metals the femtosecond optical measurements in ferromagnets are even more important. Using femtosecond Kerr-rotation measurements Beaupaire and co-workers demonstrated [54] that fs-laser induced heating of electrons resulted into the simultaneous drop in magnetization (ultrafast demagnetization) in a ferromagnetic nickel. Later on it has been shown that the demagnetization dynamics occurred within electron-electron thermalization time of about 50 fs after which the spins followed the dynamics of electronic temperature [55], as confirmed by other measurements [56]. For large density of laser excitation (fluence) of the order of a few mJ/cm² the demagnetization dynamics became even more complex and could be described by different relaxation times for electrons and spins, both in sub-100 fs time range [57].

Ultrafast decay of magnetization in Ni was contrasted by relatively slow demagnetization in Gd on a time-scale of about 100 ps [58]. Very recently the paradoxical diversity of magnetization dynamics observed in many magnetic materials was explained by different contributions to magnetization via delocalized electronic states (3d4sp states dominating in Ni) and bound states (4f states in Gd) [37]. The observation of small ultrafast component in magneto-optical Kerr measurements in Gd caused by heating of 5d6sp electrons confirmed the universal character of ultrafast demagnetization pathway by delocalized electrons.

The dynamics of magnetization recovery is governed by its precessional motion and can be adequately described by the phenomenological Landau-Lifshitz-Gilbert (LLG) equations in which the length of magnetization vector is not conserved [59]: the typical magnetization dynamics represent a damped precession with a period of several tens of picoseconds and a decay time of a few hundreds of picoseconds. Magnetocrystalline anisotropy in cobalt is found to significantly alter the trajectories of magnetization vector, an effect important in the context of studying switching dynamics [60].

Numerous studies of fs-laser induced magnetization dynamics in various ferromagnetic and antiferromagnetic materials lead to the pioneering observation that a single intense circularly polarized fs-laser pulse can deterministically switch the magnetization in a ferrimagnetic GdFeCo alloy, with the magnetization direction determined by the helicity (right- or left-handed) of circularly polarized light [61, 62]. The switching pathway could be adequately described by LLG equations for magnetization dynamics as well. Very recently this experiment was reproduced with much longer picosecond pump pulses confirming the precessional nature of magnetization switching [63]. However, the physical nature of the long-living helicity reservoir for angular momentum in the material was called into question for a following reason: the angular momentum cannot be stored long enough in short-living electronic excitations as comes out to be necessary to explain switching with picosecond laser pulses. Irrespective of the pulse duration switching occurred only when a significant amount of heat (incident laser fluence of 6 mJ/cm²) was deposited in the material. At even higher fluences the deterministic thermal magnetization switching was observed with linearly polarized light [64] suggesting that all-optical helicity-dependent reversal exists only within a relatively narrow range of fluences (within $\sim 10\%$ above the switching threshold).

F. Prospects: ultrafast acoustic magnetization switching

For practical applications it would be highly desirable to develop new ways of magnetization reversal not relying on thermal mechanisms. The proof-of-principle non-thermal magnetization reversal in Co/Pt multilayer structures

was achieved with ultrashort pulses of magnetic field $B(t)$ generated by relativistic electron bunches [65], i.e. in a large-scale facility experiment. Thinking further in terms of miniaturized ultrafast hybrid devices combining different functionalities one could imagine magnetization reversal in the magneto-plasmonic switch by means of ultrashort acoustic pulses.

The possibility of using reasonably low external stress of the order of 100 MPa as a source of an effective magnetic field $B_{eff}(t)$ for magnetization reversal in nickel nanomagnets was discussed recently [66]. The first experiments on acoustically induced magnetization dynamics in ferromagnetic semiconductor GaMnAs at cryogenic temperature revealed only minor perturbations of magnetization direction [67]. Similar room-temperature experiments in polycrystalline nickel films demonstrated much larger acoustic rotation of magnetization direction of about 4° out of the equilibrium [68].

It is likely that not only longitudinal (compressional or tensile) but also transversally polarized acoustic *shear* pulses [69] can efficiently interact with magnetization and may even contribute to the dynamics of all-optical magnetization switching [61]. Femtosecond circularly polarized light pulses may act as an ultrafast 'screwdriver': due to efficient electron-phonon coupling the directed circular surface current driven by the rotating electric field of a circularly polarized pump pulse should generate a helically polarized pulse of acoustic shear phonons acting as a source of long-living effective magnetic field $B_{eff}(t)$ in the direction normal to the surface [70]. Whether or not this hypothesis, which at least does not contradict the most recent experimental observations [63], will be confirmed in the experiment, the future of ultrafast magneto-elastic interactions looks bright.

G. BOX1: measurements with surface plasmons

When the electrons in bulk metal are displaced with respect to the ions, the (tiny) charge separation induces an electric field, which tends to restore the electrical neutrality. This relaxation process is governed by oscillations of the electrons at plasma frequency $\omega_p = \sqrt{\frac{n_e e^2}{\epsilon_0 m_{eff}}}$. Since in most metals there is at least one free electron per ion, the resulting electron density $n_e \sim 10^{22} \text{ cm}^{-3}$ is very high and $\hbar\omega_p \sim 10 \text{ eV}$. A simple Drude model for the linear dielectric susceptibility of a metal $\epsilon_m(\omega) = \epsilon_{xx}(\omega) = 1 - \omega_p^2 / (\omega(\omega + i/\tau_{Dr}))$, where τ_{Dr} stands for an effective electron scattering time, represents a reasonable approximation for the optical properties of noble free-carrier-like metals (Ag, Au, Cu, Al) in the spectral region free from interband transitions. Their relatively low optical losses due to the large electronic collision time $\tau_c \sim 10 \text{ fs}$ favor applications in plasmonics, in contrast to high-loss ferromagnetic metals (Fe, Ni, Co) characterized by $\tau_{Dr} \sim 1 \text{ fs}$. Another very important parameter, the mean free path l_e of electrons at a Fermi surface is also much larger in noble metals.

Surface plasmon polaritons (SPP or SP) exist in a broad frequency band obeying the inequality $\text{Re}[\epsilon_m(\omega)] < -1$ ($\omega < \omega_p/\sqrt{2}$) and are characterized by dispersion relation $k_{sp}(\omega) = k_0 \sqrt{\frac{\epsilon_m(\omega)}{\epsilon_m(\omega)+1}}$, where $k_0 = \omega/c$ is the wavevector of light in vacuum and k_{sp} is SP wave vector. Since $k_{sp} > k_0$ for all frequencies SP cannot be excited by plane electromagnetic waves impinging on a metal-air interface. An elegant and most widely used way to excite surface plasmons is provided by the so-called Kretschmann geometry [72] (see Fig. 6a), where a thin metal film deposited on top of a dielectric prism is illuminated by a collimated light beam through the prism with refractive index $n > 1$. For a particular combination of optical wavelength and angle of incidence Θ_0 the in-plane component of the wave vector of p-polarized incident light $k_x(\Theta) = nk_0 \sin \Theta$ becomes equal to SP wave vector, $k_{sp}(\Theta_0) = k_x(\Theta_0)$, leading to phase-matched excitation of SP at metal-air interface. The angular dependence of reflectivity $R(\theta, \lambda)$ shows a very sharp dip at $\theta = \theta_0$ with a width of about 1 degree, see Fig. 6b. Thanks to very high gradient $dR(\theta)/d\theta$ around the dip a small change Δk_{sp} in SP wave vector results in the shift in the resonant angle $\Delta\Theta$ (or optical wavelength $\Delta\lambda$) inducing a large change ΔR in reflectivity - a physical principle behind the surface plasmon resonance (SPR) sensing [22, 71].

The metal layer must be relatively thin (typically $\sim 50 \text{ nm}$) in order to allow for efficient coupling of incident light from the glass-metal to the metal-air interface [73, 74]. Incident light must be p-polarized for optimum coupling to SP: indeed, the electric fields of s-polarized beam and SP are perpendicular making their coupling impossible. Due to phase-matched excitation mechanism in Kretschmann geometry SP intensity grows upon propagation along the surface and can get up to 300 times larger as compared to the incident light intensity, depending on energy dissipation in the metal [75]. In a realistic situation the enhancement factor is lower due to other effects reducing the surface plasmon propagation length such as, for example, surface roughness [76]. This SP intensity enhancement plays a major role in the non-linear optics with surface plasmons [77] and in the generation of high-energy electrons with ultrashort SP pulses.

Another way of SP excitation is based on light scattering on metal nano-structures. The plasmonic double-slit experiment [78] triggered the development of quantitative surface plasmon interferometry [5, 7, 79, 80]. Figure 6c illustrates SP interferometry with a slit-groove arrangement in gold film. A collimated laser beam (either continuous

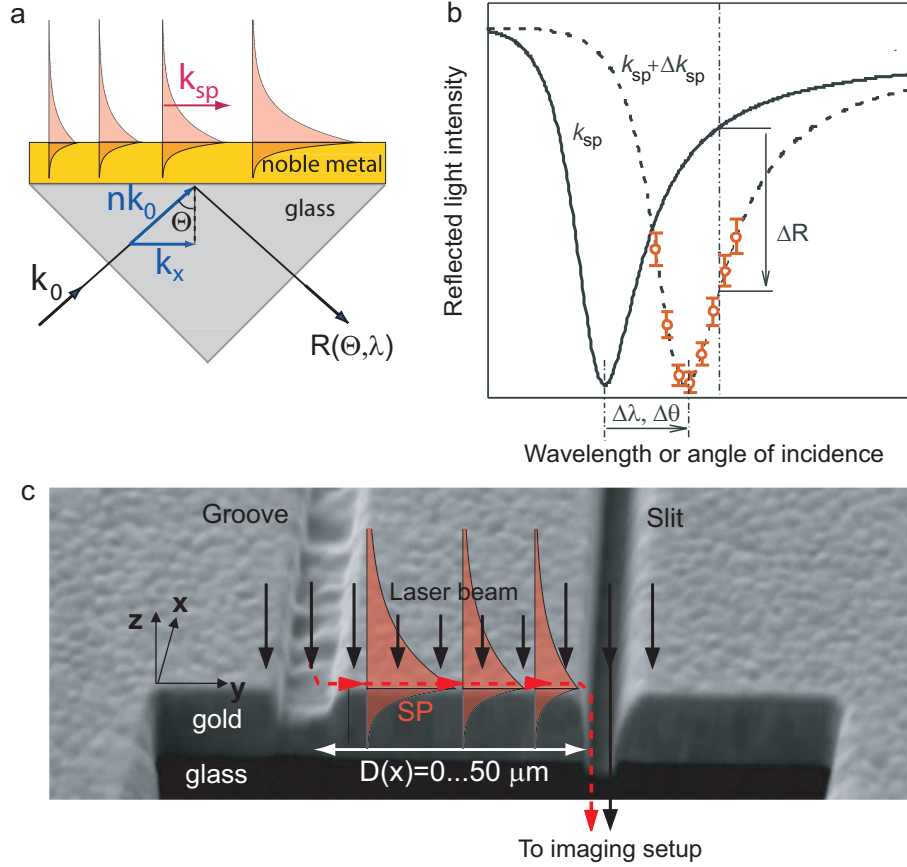


FIG. 6: **SP excitation and sensing.** **a**, Kretschmann geometry for SP excitation in a thin film of a noble metal on a dielectric prism. SP intensity grows upon propagation. **b**, A small change of SP wave vector k_{sp} induces a large change in the intensity of reflected light ΔR . **c**, Scanning electron microscopy image of a slit-groove pair milled by a focussed ion beam in a 200 nm thin gold film on glass. A 200 nm wide and 100 nm deep groove and a 100 nm wide slit are milled by the focussed ion beam. SPs are excited at the groove, propagate towards the slit where they interfere with directly transmitted light. SP intensity decays upon propagation. Figures adopted with permission from: **b**, ref. [71]; **c**, ref. [29].

or pulsed) illuminates the entire area of the microinterferometer and leads to most efficient SP excitation at a wider groove. SPs propagate in the direction perpendicular to groove axes towards the slit, where they are scattered back into free-space radiation and interfere with directly transmitted light. In case of a *tilted* groove [7, 29] the slit-groove distance $D(x)$ varies along the slit axes x resulting into the periodic modulation of light intensity transmitted through the slit. Any modulation of SP wave vector k_{sp} or propagation distance L_{sp} induce the phase shift or change in contrast of this plasmonic interference pattern, respectively, see example in Fig. 4c.

-
- [1] Gramotnev, D. K. & Bozhevolnyi, S. I. Plasmonics beyond the diffraction limit. *Nature Photon.* **4**, 83–91 (2010).
 - [2] Berini, P. & Leon, I. D. Surface plasmon-polariton amplifiers and lasers. *Nature Photon.* **6**, 16–24 (2012).
 - [3] Krasavin, A. V. & Zheludev, N. I. Controlling signals in au/ga waveguide using nanoscale structural transformations. *Appl. Phys. Lett.* **84**, 1416–1418 (2004).
 - [4] Dicken, M. J. *et al.* Electrooptic modulation in thin film barium titanate plasmonic interferometers. *Nano Lett.* **8**, 4048–4052 (2008).
 - [5] Pacifici, D., Lezec, H. J. & Atwater, H. A. All-optical modulation by plasmonic excitation of cdse quantum dots. *Nature Photon.* **1**, 402–406 (2007).
 - [6] Fedutik, Y., Temnov, V. V., Schöps, O., Woggon, U. & Artemyev, M. V. Exciton-plasmon-photon conversion in plasmonic nanostructures. *Phys. Rev. Lett.* **99**, 136802 (2007).
 - [7] Temnov, V. V. *et al.* Active magneto-plasmonics in hybrid metal-ferromagnet structures. *Nature Photon.* **4**, 107–110 (2010).

- [8] Temnov, V. V. & Woggon, U. Nanoplasmonics with colloidal quantum dots. In Tartakovskii, A. (ed.) *Quantum dots: optics, electron transport and future applications*, 185–201 (Cambridge University press, Cambridge, 2012).
- [9] Fan, S. Magnet-controlled plasmons. *Nature Photon.* **4**, 76–77 (2010).
- [10] Chiu, K. W. & Quinn, J. J. Magneto-plasma surface waves in solids. *Nuovo Cimento* **10B**, 1–20 (1972).
- [11] Haefner, P., Luck, E. & Mohler, E. Magneto-optical properties of surface plasma waves on copper, silver, gold, and aluminum. *Phys. Stat. Sol.* **185**, 289–299 (1994).
- [12] Oppeneer, P. M. & Antonov, V. N. Energy-band theory of the magneto-optical kerr effect of selected ferromagnetic materials. No. 466 in *Lecture Notes in Physics*, 29–47 (Springer, Berlin, 1995).
- [13] Krinchik, G. S. Ferromagnetic hall effect at optical frequencies and inner effective magnetic field of ferromagnetic metals. *J. Appl. Phys.* **35**, 1089–1092 (1964).
- [14] Hermann, C. *et al.* Surface-enhanced magneto-optics in metallic multilayer films. *Phys. Rev. B* **64**, 235422 (2001).
- [15] Gonzalez-Diaz, J. B. *et al.* Surface-magnetoplasmon nonreciprocity effects in noble-metal/ferromagnetic heterostructures. *Phys. Rev. B* **76**, 153402 (2007).
- [16] Ferreiro-Vila, E. *et al.* Magneto-optical and magnetoplasmonic properties of epitaxial and polycrystalline au/fe/au trilayers. *Phys. Rev. B* **83**, 205120 (2011).
- [17] Mertin-Becerra, D. *et al.* Enhancement of the magnetic modulation of surface plasmon polaritons in au/co/au films. *Appl. Phys. Lett.* **97**, 183114 (2010).
- [18] Belotelov, V. I. *et al.* Enhanced magneto-optical effects in magneto-plasmonic crystals. *Nature Nanotechn.* **6**, 370–276 (2011).
- [19] Ebbesen, T. W., Lezec, H. J., Ghaemi, H. F., Thio, T. & Wolff, P. A. Extraordinary optical transmission through sub-wavelength hole arrays. *Nature* **391**, 667 (1998).
- [20] Valev, V. K. *et al.* Plasmons reveal the direction of magnetization in nickel nanostructures. *ACS Nano* **5**, 91–96 (2011).
- [21] Regatos, D., Sepulveda, B., Farina, D., Carrascosa, L. G. & Lechuga, L. M. Suitable combination of noble/ferromagnetic metal multilayers for enhanced magneto-plasmonic biosensing. *Opt. Express* **19**, 8336–8346 (2011).
- [22] Homola, J., Yee, S. S. & Gauglitz, G. Surface plasmon resonance sensors: review. *Sens. Act. B: Chemical* **54**, 3–15 (1999).
- [23] MacDonald, K. F., Samson, Z. L., Stockman, M. I. & Zheludev, N. I. Ultrafast active plasmonics. *Nature Photon.* **3**, 55–58 (2008).
- [24] Tas, G. & Maris, H. J. Electron diffusion in metals studied by picosecond ultrasonics. *Phys. Rev. B* **49**, 15046 (1994).
- [25] Samson, Z. L., MacDonald, K. F. & Zheludev, N. I. Femtosecond active plasmonics: ultrafast control of surface plasmon propagation. *J. Opt. A* **11**, 1–4 (2009).
- [26] Rotenberg, N., Betz, M. & van Driel, H. M. Ultrafast all-optical coupling of light to surface plasmon polaritons on plain metal surfaces. *Phys. Rev. Lett.* **105**, 017402 (2010).
- [27] Fatti, N. D. *et al.* Nonequilibrium electron dynamics in noble metals. *Phys. Rev. B* **61**, 16956–16966 (2000).
- [28] Thomsen, C., Grahn, H. T., Maris, H. J. & Tauc, J. Surface generation and detection of phonons by picosecond light pulses. *Phys. Rev. B* **34**, 4129–4138 (1986).
- [29] Temnov, V. V. *et al.* Femtosecond surface plasmon interferometry. *Opt. Express* **17**, 8423–8432 (2009).
- [30] van Exter, M. & Lagendijk, A. Ultrashort surface-plasmon and phonon dynamics. *Phys. Rev. Lett.* **60**, 49–52 (1988).
- [31] Siemens, M. E. *et al.* Quasi-ballistic thermal transport from nanoscale interfaces observed using ultrafast coherent soft x-ray beams. *Nature. Mater.* **9**, 26–30 (2010).
- [32] Wang, J., Wu, J. & Guo, C. Resolving dynamics of acoustic phonons by surface plasmons. *Opt. Lett.* **32**, 719–721 (2007).
- [33] Wang, J. & Guo, C. Effect of electron heating on femtosecond laser-induced coherent acoustic phonons in noble metals. *Phys. Rev. B* **75**, 184304 (2007).
- [34] Perner, M. *et al.* Observation of hot-electron pressure in the vibration dynamics of metal nanoparticles. *Phys. Rev. Lett.* **85**, 792–795 (2000).
- [35] Groeneveld, R. H. M., Sprik, R. & Lagendijk, A. Ultrafast relaxation of electrons probed by surface plasmons at a thin silver film. *Phys. Rev. Lett.* **64**, 784 (1990).
- [36] Temnov, V. V. *et al.* Femtosecond nonlinear ultrasonics in gold probed with ultrashort surface plasmons. (*to be published*)
- [37] Koopmans, B. *et al.* Explaining the paradoxical diversity of ultrafast laser-induced demagnetization. *Nature. Mater.* **9**, 259–265 (2010).
- [38] Getzlaff, M., Bansmann, J. & Schönhense, G. Spin-polarization effects for electrons passing through iron and cobalt films. *Solid. State. Comm.* **87**, 467–469 (1993).
- [39] Crowell, C. R., Spitzer, W. G., Howarth, L. E. & LaBate, E. E. Attenuation length measurements of hot electrons in metal films. *Phys. Rev.* **127**, 2006–2014 (1962).
- [40] Saito, T., Matsuda, O. & Wright, O. B. Picosecond acoustic phonon pulse generation in nickel and chromium. *Phys. Rev. B* **67**, 205421 (2003).
- [41] Hao, H. Y. & Maris, H. J. Experiments with acoustic solitons in crystalline solids. *Phys. Rev. B* **64**, 064302 (2001).
- [42] van Capel, P. J. S. & Dijkhuis, J. I. Time-resolved interferometric detection of ultrafast strain solitons in sapphire. *Phys. Rev. B* **81**, 144106 (2010).
- [43] Devos, A. & Lerouge, C. Evidence of laser-wavelength effect in picosecond ultrasonics: possible connection with interband transitions. *Phys. Rev. Lett.* **86**, 2669–2672 (2003).
- [44] Cai, W., Hofmeister, H. & Dubiel, M. Importance of lattice contraction in surface plasmon resonance shift for free and embedded silver nanoparticles. *E. Phys. J. D* **13**, 245–253 (2001).

- [45] Lerne, J. *et al.* Influence of lattice contraction on the optical properties and the electron dynamics in silver clusters. *E. Phys. J. D* **17**, 213–220 (2001).
- [46] Devos, A. & Louarn, A. L. Strong effect of interband transitions in the picosecond ultrasonics response of metallic thin films. *Phys. Rev. B* **68**, 045405 (2003).
- [47] Temnov, V. V., Sokolowski-Tinten, K., Zhou, P. & von der Linde, D. Ultrafast imaging interferometry at femtosecond laser-excited surfaces. *J. Opt. Soc. Am. B* **23**, 1954 (2006).
- [48] Ruppert, C. *et al.* Surface acoustic wave mediated coupling of free-space radiation into surface plasmon polaritons on plain metal films. *Phys. Rev. B* **82**, 081416 (2011).
- [49] Irvine, S. E., Dechant, A. & Elezzabi, A. Y. Generation of 0.4-keV femtosecond electron pulses using impulsively excited surface plasmons. *Phys. Phys. Lett.* **93**, 184801 (2004).
- [50] Zawadzka, J., Jaroszynski, D. A., Carey, J. J. & Wynne, K. Evanescent-wave acceleration of femtosecond electron bunches. *Nucl. Instr. Meth. Phys. Research A* **455**, 324–328 (2000).
- [51] Racz, P. *et al.* Strong-field plasmonic electron acceleration with few-cycle, phase-stabilized laser pulses. *Appl. Phys. Lett.* **98**, 111116 (2011).
- [52] Welsh, G. H. & Wynne, K. Generation of ultrafast terahertz radiation pulses on metallic nanostructured surfaces. *Opt. Express* **17**, 2470–2480 (2009).
- [53] Kadlec, F., Kuzel, P. & Coutaz, J. L. Study of terahertz radiation generated by optical rectification on thin gold films. *Opt. Lett.* **30**, 1402–1404 (2005).
- [54] Beaurepaire, E., Merle, J. C., Daunois, A. & Bigot, J.-Y. Ultrafast spin dynamics in ferromagnetic nickel. *Phys. Rev. Lett.* **76**, 4250–4253 (1996).
- [55] Guidoni, L., Beaurepaire, E. & Bigot, J.-Y. Magneto-optics in the ultrafast regime: thermalization of spin populations in ferromagnetic films. *Phys. Rev. Lett.* **89**, 017401 (2002).
- [56] Güdde, J., Conrad, U., Jähne, V., Hohlfeld, J. & Matthias, E. Magnetization dynamics of Ni and Co films on Cu(001) and of bulk nickel surfaces. *Phys. Rev. B* **59**, R6608 (1999).
- [57] Bigot, J.-Y., Vomir, M., & Beaurepaire, E. Coherent ultrafast magnetism induced by femtosecond laser pulses. *Nature Phys.* **5**, 515–520 (2009).
- [58] Vaterlaus, A., Beutler, T. & Meier, F. Spin-lattice relaxation time of ferromagnetic gadolinium determined with time-resolved spin-polarized photoemission. *Phys. Rev. Lett.* **67**, 2214–3317 (1991).
- [59] Vomir, M., Andrade, L. H. F., Guidoni, L., Beaurepaire, E. & Bigot, J.-Y. Real space trajectory of the ultrafast magnetization dynamics in ferromagnetic metals. *Phys. Rev. Lett.* **94**, 237601 (2005).
- [60] Bigot, J.-Y., Vomir, M., Andrade, L. H. F. & Beaurepaire, E. Ultrafast magnetization dynamics in ferromagnetic cobalt: the role of anisotropy. *Chem. Phys.* **76**, 137–146 (2005).
- [61] Stanciu, C. D. *et al.* All-optical magnetic recording with circularly polarized light. *Phys. Rev. Lett.* **99**, 047601 (2007).
- [62] Vahaplar, K. *et al.* Ultrafast path for optical magnetization reversal via a strongly nonequilibrium state. *Phys. Rev. Lett.* **103**, 117201 (2009).
- [63] Steil, D., Alebrand, S., Hassdenteufel, A., Cinchetti, M. & Aeschlimann, M. All-optical magnetization recording by tailoring optical excitation parameters. *Phys. Rev. B* **84**, 224498 (2011).
- [64] Ostler, T. A. *et al.* Ultrafast heating as a sufficient stimulus for magnetization reversal in a ferrimagnet. *Nature Commun.* **3**, 1–6 (2012).
- [65] Back, C. H. *et al.* Magnetization reversal in ultrashort magnetic field pulses. *Phys. Rev. Lett.* **81**, 3251–3254 (1998).
- [66] Atulasimha, J. & Bandyopadhyay, S. Bennett clocking of nanomagnetic logic using multiferroic single-domain nanomagnets. *Appl. Phys. Lett.* **97**, 173105 (2010).
- [67] Scherbakov, A. V. *et al.* Coherent magnetization precession in ferromagnetic (Ga,Mn)As induced by picosecond acoustic pulses. *Phys. Rev. Lett.* **105**, 117204 (2010).
- [68] Kim, J. W., Vomir, M. & Bigot, J.-Y. Ultrafast magneto-acoustics in nickel films. *arXiv:1201.0170v1* (2012).
- [69] Pezeril, T., Klieber, C., Andrieu, S. & Nelson, K. A. Optical generation of gigahertz-frequency shear acoustic waves in liquid glycerol. *Phys. Rev. Lett.* **102**, 107402 (2009).
- [70] de la Fuente, C. *et al.* Magnetocrystalline anisotropy in a (110) (Tb_{0.27}Dy_{0.73})Fe₂ thin-film. *J. Phys. Condens. Mat.* **16**, 2959–2966 (2004).
- [71] Piliarik, M. & Homola, J. Surface plasmon resonance (SPR) sensors: approaching their limits? *Opt. Express* **17**, 16505–16517 (2009).
- [72] Kretschmann, E. & Raether, H. Radiative decay of nonradiative surface plasmons excited by light. *Z. Naturforsch. A* **23**, 2135–2136 (1968).
- [73] Fukui, M., So, V. C. Y. & Normandin, R. Lifetimes of surface plasmons in thin silver films. *Phys. Stat. Sol.* **91**, K61–K64 (1979).
- [74] Sarid, D. Long-range surface-plasma waves on very thin metal films. *Phys. Rev. Lett.* **47**, 1027–1930 (1981).
- [75] Weber, W. H. & Ford, G. W. Optical electric-field enhancement at a metal surface arising from surface-plasmon excitation. *Opt. Lett.* **6**, 122 (1981).
- [76] Nagpal, P., Lindquist, N. C., Oh, S. H. & Norris, D. J. Ultrasoft patterned metals for plasmonics and metamaterials. *Science* **325**, 594–597 (2009).
- [77] Grosse, N. B., Heckmann, J. & Woggon, U. Nonlinear plasmon-photon interaction resolved by k-space spectroscopy. *Phys. Rev. Lett.* **108**, 136802 (2012).
- [78] Schouten, H. F. *et al.* Plasmon-assisted two-slit transmission: Young’s experiment revisited. *Phys. Rev. Lett.* **94**, 053901 (2005).

- [79] Gay, G. *et al.* The response of nanostructured surfaces in the near field. *Nature Phys.* **2**, 262 (2006).
- [80] Temnov, V. V., Woggon, U., Dintinger, J., Devaux, E. & Ebbesen, T. W. Surface plasmon interferometry: measuring group velocity of surface plasmons. *Opt. Lett.* **32**, 1235 (2007).

Correspondence

Correspondence and requests for materials should be addressed to V.T. (email: vasily.temnov@univ-lemans.fr).